Environmental Science and Pollution Research (2021) 28:45879–45890
https://doi.org/10.1007/s11356-021-13937-z

RESEARCH ARTICLE

Long-term exposure to low doses of aluminum affects mineral content and microarchitecture of rats alveolar bone

Deiweson Souza-Monteiro[1] · Railson de Oliveira Ferreira[1] · Luciana Guimarães Eiró[1] · Leidiane Alencar de Oliveira Lima[1] · Gabriela Souza Balbinot[2] · Simone Patricia Aranha da Paz[3] · Alan Rodrigo Leal Albuquerque[3] · Fabricio Mezzomo Collares[2] · Rômulo Simões Angélica[3] · Sofia Pessanha[4] · Cristiane do Socorro Ferraz Maia[5] · Rafael Rodrigues Lima[1]

Received: 15 December 2020 / Accepted: 9 April 2021 / Published online: 21 April 2021

Abstract

Aluminum (Al) is one of the most found elements in nature in many forms, and human exposure can be quite common. Therefore, it is important to investigate the effects of exposure to Al mainly at low doses and for a prolonged period, in order to simulate human exposure in the periodontium, an important structure for support and protection of the teeth. This investigation aimed to study the aluminum chloride ($AlCl_3$) toxicological effects in the mineral composition and micromorphology of the alveolar bone of rats. Two groups of eight male Wistar rats were used for the experiment. $AlCl_3$ group was exposed to $AlCl_3$ orally at a dose of 8.3 mg/kg/day for 60 days, while the control group received only distilled water. After that, the mandibles were collected and submitted to the following analyses: Fourier transform infrared spectroscopy, Raman spectroscopy, and X-ray microtomography analysis; blood was also collected for determination of Al circulating levels. Our data showed that $AlCl_3$ was capable of increasing Al circulating levels in blood. It was able to promote changes in the mineral content and triggers significant changes in the mineralized bone microstructure, such as number and thickness of trabeculae, being associated with alveolar bone-loss.

Keywords Aluminum chloride · Toxicology · Alveolar bone · Raman spectroscopy · MicroCT · Bone loss

Introduction

Widespread presence of aluminum (Al) is well-known, as this metal is one of the most common elements on Earth, and due to its high affinity for oxygen and metals, many chemical compounds can be formed (Kumar and Gill 2014; Goulléa and Grangeot-Keros 2019). Even though it is very common, Al does not seem to have any important role in human and animal biology (Bondy 2016).

Many applications have been attributed to uses of Al in our society (Chappard et al. 2016). The addition of Al salts in vaccines to provoke a stronger immune response and help vaccine dynamic is an adjuvant technique used over the years all around the world (Gherardi et al. 2016; Lin et al. 2018; Principi and Esposito 2018). Al is also used in large scale in transport, construction, packing, and machine industries (Chappard et al. 2016; Lewis et al. 2014; Nie 2018) due to its high resistance, ductility, and capacity to conduct energy and heat (Hirshi 2006; Totten and Mackenzie 2003).

Responsible Editor: Mohamed M. Abdel-Daim

✉ Rafael Rodrigues Lima
rafalima@ufpa.br

1 Laboratory of Functional and Structural Biology, Institute of Biological Sciences, Federal University of Pará, Augusto Corrêa, n1, Belém 66075-110, Pará, Brazil

2 Dental Material Laboratory, School of Dentistry, Federal University of Rio Grande do Sul, Porto Alegre, Rio Grande do Sul, Brazil

3 Laboratory of X-Ray Diffraction, Institute of Geosciences, Federal University of Pará, Belém, Pará, Brazil

4 Laboratory of Instrumentation, Biomedical Engineering and Radiation Physics, NOVA School of Science and Technology, Campus Caparica, 2829-516 Caparica, Portugal

5 Laboratory of Pharmacology of Inflammation and Behavior, Faculty of Pharmacy, Institute of Health Science, Federal University of Pará, Belém, Pará, Brazil

Moreover, Al is used in food additives (e.g., E173, E523) (ESFA 2013; Chappard et al. 2016) and in water purification (Kumar and Gill 2014) bringing the gastric absorption to the debate. Previous investigation showed that Al is absorbed in all forms of exposure (Exley 2013; Ligt et al. 2018) and easily enters the human body by combining the Al ion with other soluble ions that can be absorbed through the human stomach with daily exposure (Yokel et al. 2008; Bojórquez-Quintal et al. 2017).

Al exposure can be also associated with environment contamination (Driscoll and Schecher 1990). Rivers and lakes may be contaminated by Al particles through sediments erosion, mainly when the pH is favorable. Acid rain is another source of exposure due to the solubilization of soil minerals with Al content, which is highly associated with Al and iron (Fe) involvement (Driscoll and Schecher 1990; Niu 2018).

Studies have already discussed Al toxicity potential associated with many biological systems damages such as the renal and central nervous system (Shirley and Lote 2005; Becaria et al. 2006; Sharma et al. 2013; Willhite et al. 2014; Klotz et al. 2017), but little is known about the toxicity of Al in the oral cavity. Oxidative imbalance and morphological changes in salivary glands had already been observed after Al chronic exposure in animals (Costa et al. 2014; Souza-Monteiro et al. 2020). However, there are no studies in the literature involving Al toxycodynamic and its effects in the periodontium, an important set of structures in the stomatognathic system.

The alveolar bone (AB) is part of the periodontium and along with periodontal fibers and cementum provides the structural support for the teeth (Chu et al. 2014; Goudouri et al. 2017). AB is a highly mineralized tissue, and its mineral content is mostly poorly crystalline hydroxyapatite due to the incorporation of other elements, such as carbonate, zinc, and magnesium ions (Goudouri et al. 2017). In pathological conditions of the periodontium, the AB loss can occur, leading to tooth loss (Kinane et al. 2017).

In this perspective, $AlCl_3$ could be used to assess the Al exposure in the alveolar bone of rats at doses that are equivalent to those considered as a dietary consumption for humans. The dose was defined in accordance with the Agency for Toxic Substances and Disease Registry, selecting factor 3 for extrapolation from human to animal, and it was about 0.16 mg of Al/kg/day (ATSDR 2006). Our study aimed to analyze the Al exposure at low dose and long-term experimental model in a structure inside the oral cavity, AB, as it displays important roles to the whole stomatognathic system homeostasis.

Material and methods

Biological model

Sixteen male Wistar rats (*Rattus norvegicus*, 35 days old) were obtained from the Federal University of Pará (UFPA, Belém, Brazil), following all the NIH Guide for the Care and Use of Laboratory Animal, and the study was approved by Ethics Committee on Experimental Animals of Federal University of Pará (under license number CEUA-UFPA 5923210617). The animals were maintained in collective cages with 4 animals each. The animals received water ad libitum, balanced pelleted food (Presence, Neovia, Brazil), and were housed under standard conditions (25 °C and 12 h dark/light cycle). All experimental steps are summarized in Fig. 1.

Experimental groups and exposure procedure

The animals were divided into control group and intoxicated group using a simple randomization, each one with eight animals. The intoxicated group received $AlCl_3$ (8.3 mg/kg) with distilled water as the vehicle by intragastric gavage for 60 days. The dose was set in accordance with the dietary consumption of Al for humans per day (0.16 mg/kg) (ATSDR 2006), and an extrapolation based on the surface body area was used (for details, see online resource 1) (Reagan-Shaw et al. 2008; Martinez et al. 2016). The animals were weighted weekly, and dose adjustment was made when necessary. The control group received only distilled water following the same protocol of the exposed group.

Sample collection

After 60 days of exposure, the animals were euthanized through intraperitoneal injection of 10% ketamine hydrochloride (90 mg/kg) and 2% xylazine hydrochloride (9 mg/kg). Blood (5 mL) was collected individually via cardiac puncture and stored in plastic vials containing the anticoagulant heparin (one drop to each mL of blood); mandibles were collected and divided for different analyses. Left hemi mandibles were stored in − 20 °C refrigerator for mineral content analyses, and right hemi mandibles were maintained in 4% formol solution for X-ray computed tomography (MicroCT) evaluation.

Blood aluminum concentration

The blood samples were lyophilized with the aid of a freeze-dryer model L 101 (Liotop, São Carlos, Brazil). The sample mass was then digested with dilute nitric acid (HNO_3) and hydrogen peroxide (H_2O_2) in a cavity microwave oven (START E, Milestone) at 200 °C for 25 min. A volume of approximately 20 μL of the digested sample was introduced into the graphite furnace atomic absorption spectrometer for the quantification of Al. All samples were analyzed in triplicate. The accuracy of the method was evaluated using the addition and recovery test. Concentrations of 12–20 μg/L were added in the digested samples, and thus, Al recoveries were obtained, and the results were expressed in μg/L.

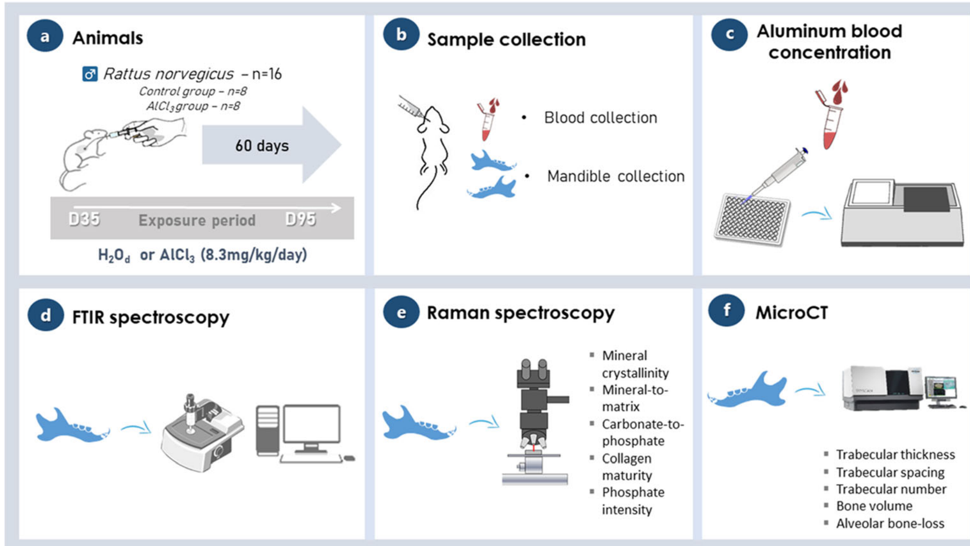

Fig. 1 Methodological steps of the study. **a** Description of experimental groups and exposure to aluminum chloride ($AlCl_3$). **b** After the exposure period, the animals were euthanized, and samples were collected. **c** Blood collection for measurement of total aluminum levels. Spectroscopics analyses for bone characterization in (**d**) and (**e**). **f** Microtomographic evaluation of alveolar bone

Sample preparation for physicochemical analyses

A section of 1 mm of the left hemi mandibles was delimited between the mesial groove and the distal groove of the first molar crown. Then, the samples were submitted to a low-speed precision cutter (IsoMet, Buehler), and the section was ready for the Raman spectroscopy analysis. The remaining alveolar bone of the first molar was submitted to the Fourier transform infrared (FTIR) spectroscopy. For this, the samples were macerated until fine granulation powder was obtained, and then they were stored in different microtubes.

FTIR spectroscopy applied to bone characterization

As a pre-treatment, the samples were dried at 60 °C for 24 h. The infrared spectra of the samples were obtained by attenuated total reflectance (ATR), using a spectrometer (Nicolet iS50 FT-IR, Thermo Scientific, USA) in the spectral region of 4000–400 cm^{-1}, with 100 scans, and resolution of 4 cm^{-1}. Data acquisition was performed using the OMNIC software.

Raman spectroscopy

The Raman mapping was performed in the inter-radicular alveolar bone of the sample in a standard area (300 × 300μm; equidistant points measured at each 100 μm) by a spectrometer (SENTERRA, Bruker Optics, Germany),

The quantification of chemical parameters was performed using XploRA Raman microscope (Horiba, France) in a near infrared laser (785 nm) with 1200 lines/mm grating. The spectral range investigated was from 300 to 1800 cm^{-1} with spectral resolution of 4 cm^{-1}. Using an entrance slit of 100 μm and a confocal hole of 300 μm, the scattered light collected by the objective was dispersed into the air-cooled CCD array of an Andor iDus detector. An × 100 objective (NA = 0.9) was used to focus in the bone surface, as well as a 50% neutral density filter rendering an incident power in the sample of 5.0 ± 0.4 mW (lasercheck®, Edmund optics).

Each spectrum was obtained by 4 accumulations of 25 seconds each, and an average of 9 measurements was performed for each sample. Spectra analysis has been performed using the software LabSpec (v5.58.25, Horiba, France), making use of a polynomial baseline correction to remove the background due to fluorescence.

The bands of interest investigated in the Raman analysis were the symmetric stretching vibration of phosphate (PO_4^{3-}) at 960 cm^{-1}, symmetric stretching of carbonate at 1070 cm^{-1}, and the broadband of the collagen related Amide I centered at 1660 cm^{-1} and 1690 cm^{-1}, and they were determined by fitting a Voigt profile to the bands (Carden and Morris 2000; Morris and Mandair 2010). Quantifications of these Raman bands were used to evaluate the mineral crystallinity, which reflects the optimal distribution of different crystal sizes and shape, and it is calculated as the inverse of full-width half-maximal (FWHM) of the band at 960 cm^{-1}. Mineral-to-matrix ratio is calculated by dividing the phosphate band by the Amide I band (1660 cm^{-1}) and indicates the amount of mineral to the organic matrix. Carbonate-to-phosphate ratio is calculated as the carbonate band divided by the phosphate band and reflects the carbonate substitution. Collagen maturity is calculated by dividing the areas of Amide I band reflecting the reducible and non-reducible collagen cross-links (Morris and Mandair 2010; Chappard et al. 2018; Khalid et al. 2018).

To graphically represent mineral content, the intensity of the PO_4^{3-} was used for the assessment of the amount of phosphate present in the area. The results were processed to obtain digitalized images of the phosphate deposition using the Sigma Plot version 12.0 for Windows software program (Systat Software Inc., San Jose, CA, USA), being performed a descriptive analysis of the levels of phosphate present in the alveolar bone region of the experimental groups through the intensity of the colors obtained in the images (Balbinot et al. 2019b).

X-ray computed microtomography

Samples were evaluated by X-ray computed microtomography (MicroCT.SMX-90 CT; Shimadzu Corp., Kyoto, Japan). Each hemi mandible was mounted in a rotary stage, where images were taken in a 360° rotation with a 70 kV intensity and 100 mA. The images were then reconstructed in the inspeXio SMX-90CT software program (Shimadzu Corp., Kyoto, Japan), with a 14 μm voxel size in images with a 1024 × 1024-pixel resolution and a 14 μm thickness, which resulted in 541 images per sample.

Measurements were performed in an image software program (ImageJ; National Institutes of Health, Bethesda, MD, USA), where images were used for the assessment of bone microarchitecture. The measurements were performed by one trained examiner, which was submitted to an interclass correlation coefficient (ICC) test, prior to the analyses. The analyses were performed in a selected stack of 50 images comprising the first lower molar alveolar bone. An area was standardized to create a region of interest (ROI), considering the inter-radicular region in the first molar starting from the coronal to the apical portion with an area of 0.300 mm^2.

A color threshold was applied to the segmentation of different grey values in the images considering the differences in bone and the other structures in the images. Based on these, the threshold was set in at 120 to 255. Trabecular thickness (Tb.Th), trabecular spacing (Tb.Sp), trabecular number (Tb.N), and bone volume in total volume (BV/TV) were measured with BoneJ plugin (Doube et al. 2010; Fernandes 2014; Balbinot et al. 2019a).

3D reconstructions of the hemi mandible were obtained using the RadiAnt DICOM Viewer 5.0.1 (Medixant, Poznan, Poland) software. The models were settled in a standard position (i.e., lingual and buccal tooth face visible). Thereby, the vertical bone loss was measured by the estimation of the cementum-enamel junction (CEJ), and the alveolar bone crest (ABC) distance was evaluated at six points of the first inferior molar (i.e., mesiolingual, midlingual, distolingual, mesiobuccal, midbuccal, distobuccal), calculating the average of these regions (Dai et al. 2015).

Statistical analyses

Statistical comparison of body weight gains between control and $AlCl_3$ groups was performed using one-way analysis of variance (ANOVA). The values obtained from the blood quantification, Raman spectroscopy, and MicroCT analysis were plotted on GraphPad Prism 7.0 software (San Diego, CA, USA) and were submitted to normality evaluation with the Shapiro-Wilk method and then compared by Student's t test with a significance level of $p < 0.05$. The results were expressed as percentage of control and mean ± SEM. The test power was calculated using the difference between the "groups" averages with the OpenEpi software (Version 2.3.1), considering the type I error of 5% and a power of 80%.

Results

Body weight measurement and Al concentration on blood

Although an expected increase in body mass was observed after the 60 days of experiments, no difference was observed at the final weight between the groups (Fig. 2a). Our results also showed, after the 60^{th} day of exposure to $AlCl_3$, that animals exposed to $AlCl_3$ presented a significantly higher Al concentration in circulating blood (83.24 ± 13.65 μg/L) when compared to the control animals (13.29 ± 3.52 μg/L) (p = 0.008) (Fig. 2b).

$AlCl_3$ modulates a response in hydroxyapatite crystals lattice

The FTIR results are illustrated in Fig. 3, where the vibrational frequency peaks are shown. In a comparative analysis between the peaks of both experimental groups, the $AlCl_3$ exposure resulted in a different spectra pattern in alveolar bone. The peaks around 1660 and 1240 cm^{-1}, corresponding to Amide I (C=O stretch) and Amide III (C-N stretch and N-H in plane bend), respectively, exhibited a lower absorbance in the $AlCl_3$ exposed group. About mineral content, in the range from 1200 to 550 cm^{-1}, corresponding to phosphate groups and carbonate peaks (Paschalis et al. 2011), was also observed a lower absorbance in the $AlCl_3$ exposed group.

$AlCl_3$ exposure changes the nanostructure and triggers alterations in mineral and inorganic content of alveolar bone

Our work revealed that Al was able to modulate a response in the mineral content of the alveolar bone in the furcation region of the exposed rats, reducing the presence of the phosphate component, as shown in Fig. 4a and b. Besides that, spatial distribution graphic, relevant ratios about bone components were evaluated through Raman spectral data.

The mineral crystallinity increased in $AlCl_3$ exposed bone when compared to control bone (control, 0.050 ± 0.0003; $AlCl_3$, 0.058 ± 0.0005; $p < 0.0001$) (Fig. 4c). In addition, significant increase of mineral-to-matrix ratio (control, 3.6 ± 0.36; $AlCl_3$, 5.8 ± 0.38; p = 0.0068) and carbonate-to-

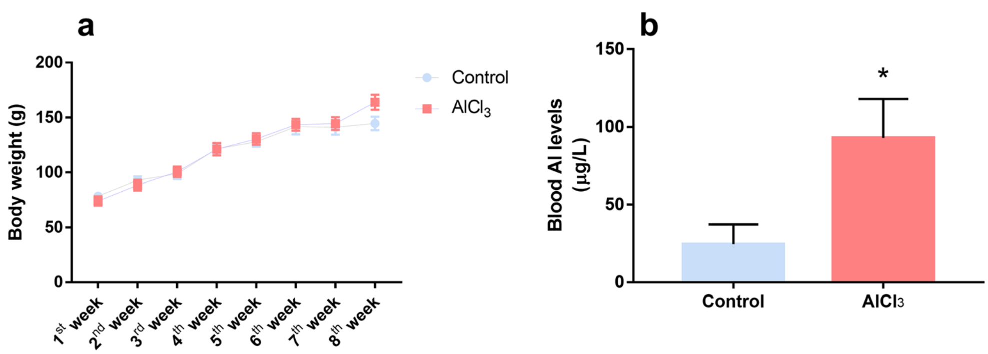

Fig. 2 Effects of $AlCl_3$ exposure on body weight and Al blood levels of rats. **a** Effects of $AlCl_3$ exposure (8.3 mg/kg/day) during 60 days on body weight (g) of rats. Results are expressed as mean ± standard error of the mean. One-way ANOVA and Tukey's post hoc test. **b** Effects of $AlCl_3$ exposure (8.3 mg/kg/day) during 60 days on total Al levels in the blood of rats (µg/L). Results are expressed as mean ± SEM Student's *t* test, $*p < 0.05$

phosphate ratio (control, 0.15 ± 0.019; $AlCl_3$, 0.21 ± 0.006; $p = 0.0267$) were observed in $AlCl_3$ samples (Fig. 4d and e, respectively). The only ratio that did not show significant difference between experimental groups was the collagen maturity (control, 9.25 ± 2.83; $AlCl_3$, 7.16 ± 2.37; $p = 0.5864$) (Fig. 4f).

Aluminum chloride exposure affects alveolar bone quality by causing damage in the alveolar bone microarchitecture

In this study, our MicroCT data showed changes in the alveolar bone micromorphology of rats exposed to $AlCl_3$ when compared to non-exposed rats (Fig. 5). Tb.Th showed a significant reduction in $AlCl_3$ exposed animals (control, 0.22 ± 0.006 mm; $AlCl_3$, 0.20 ± 0.007 mm; $p = 0.0463$). $AlCl_3$ exposure also promoted decrease in Tb.N (control, 5.18 ± 0.17 1/mm; $AlCl_3$, 4.59 ± 0.12 1/mm; $p = 0.0242$) and in BV/TV (control, 0.33 ± 0.02 %; $AlCl_3$, 0.21 ± 0.01 %; $p = 0.0012$) of AB. In the Tb.Sp parameter, a significant increase was observed in AB after $AlCl_3$ chronic exposure (control, 0.20 ± 0.004 mm; $AlCl_3$, 0.24 ± 0.010 mm; $p = 0.0047$).

$AlCl_3$-induced toxicity promoted alveolar bone-loss

The results of Fig. 6 show the measurements between the cementum-enamel junction to alveolar bone crest (CEJ-ABC). The aluminum exposed group presented increased values (control, 0.85 ± 0.007 mm; $AlCl_3$, 0.96 ± 0.013 mm; $p < 0.0001$) when compared to the control.

All statistical differences mentioned exhibited a power of the test above of 80%. For all the mean, standard deviation, standard error of the mean, and test power values of each analysis, see online resource 2.

Fig. 3 FTIR spectra of the experimental samples. Purple color represents vibrational data of control group, and red color represents vibrational data of $AlCl_3$ group (8.3 mg/kg/day during 60 days)

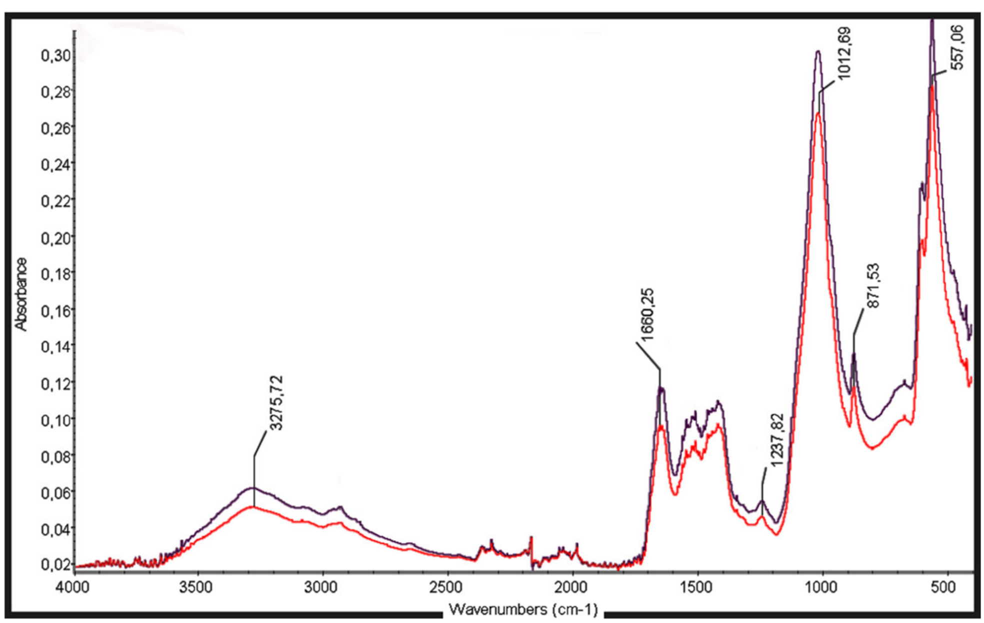

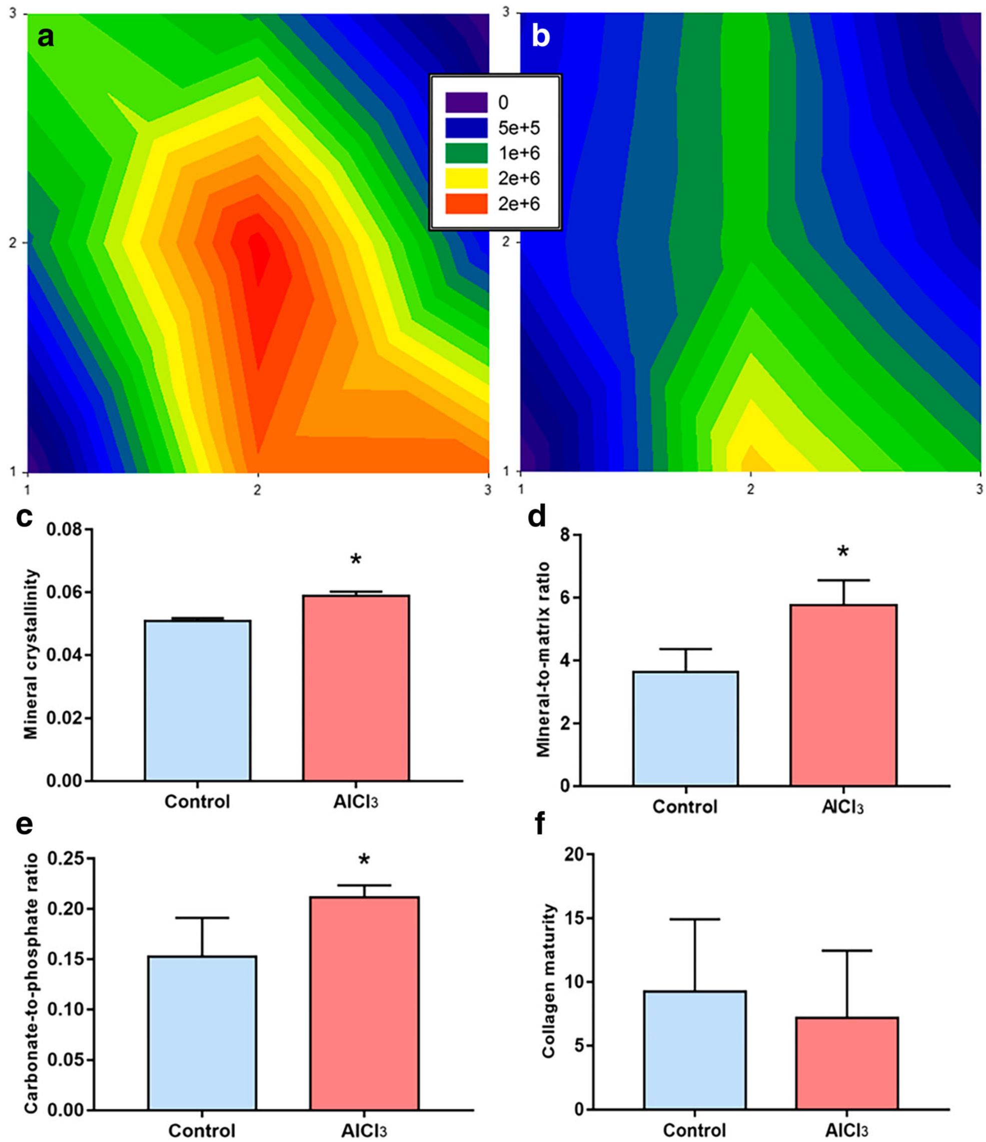

Fig. 4 Effects of $AlCl_3$ exposure (8.3 mg/kg/day) during 60 days on the organic and inorganic content of experimental rats alveolar bone. Colorimetric graphics (**a**,**b**) represent control group and aluminum group, respectively. Higher intensities are represented by red/yellow/green and blue regions represent lower or total absence of phosphate intensity. **c** Mineral crystallinity ratio; **d** mineral-to-matrix ratio; **e** carbonate-to-phosphate ratio, and **f** collagen maturity ratio. Results are expressed as mean ± SEM. Student's *t* test, $*p < 0.05$

Discussion

Our study showed evidences that $AlCl_3$ exposure, in low doses and during a chronic period, modulates alterations in the hydroxyapatite crystals and in the organic content of the alveolar bone. Changes in the alveolar bone micromorphology were observed after the exposure, and $AlCl_3$ aggravated the spontaneous alveolar bone loss in rats associated with alterations on bone matrix content.

Environmental exposure to Al has been reported and associated with Al-induced diseases (Cheng 2016). Since this metal is present in a ubiquitous form on Earth, Al exposure is almost inevitable, and studies towards its effects are necessary (Nie 2018). Human exposure is a recurrent process as the metal can be present in the air or soil by natural phenomena, and it is widely used in the industry (Chappard et al. 2018; Niu 2018). The establishment of the dose used in this study was made to simulate daily consumption in rats (Carden and Morris 2000), using the extrapolated dose method based on differences between rodents and humans.

This allometric calculation took into account the different weights, metabolisms, body surface areas, and excretion mechanisms (Reagan-Shaw et al. 2008). Oral gavage was used to ensure the Al consumption in a precise individually exposure. The method accuracy was validated as a higher concentration of Al was seen on exposed animals, without mortality and significant alterations on weight between the experimental groups.

The Al main route of elimination is the urine, and studies already have shown that renal dysfunction is a major issue for Al accumulation in the body (Salusky et al. 1991; Schifman and Luevano 2018), and patients with renal insufficiency are susceptible to anemia and bone diseases (Colomina and Peris-Sampedro 2017). One of the explanations for this issue is the

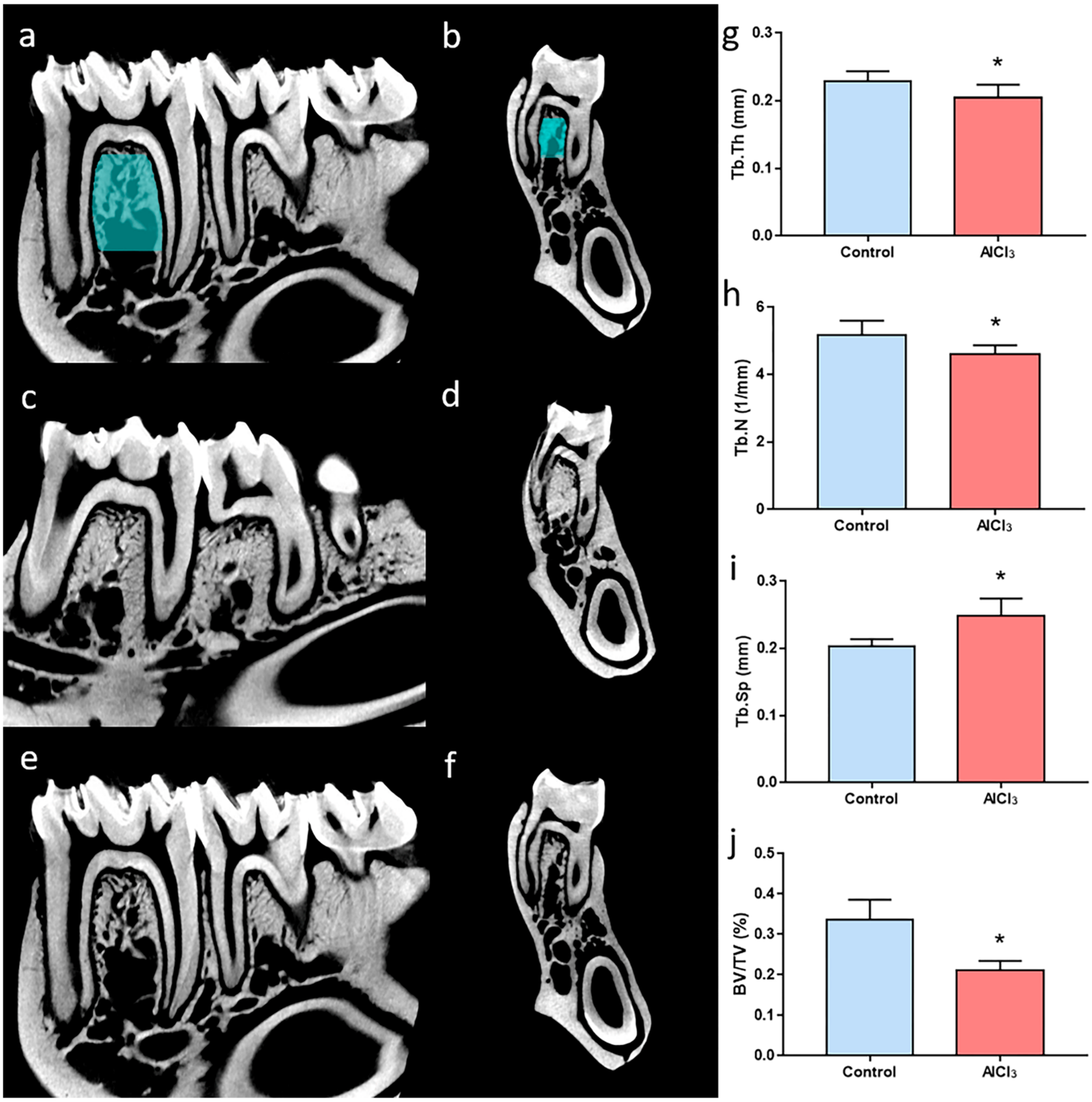

Fig. 5 Effects of $AlCl_3$ exposure (8.3 mg/kg/day) during 60 days on the alveolar bone quality of rats. In (**a**) and (**b**), sagittal and coronal slices of the animals hemi-mandibles with the region of interest to microarchitecture parameters analyze in blue. In (**c**) and (**d**), a representative sample of the control group, and in (**e**) and (**f**) a representative sample of the aluminum group. **g** Trabecular thickness (mm); **h** trabecular number (1/mm); **i** trabecular spacing (mm); and **j** bone volume (%). Results are expressed as mean ± SEM. Student's *t* test, $^*p < 0.05$

protein-bind complexes that Al makes in the plasma (Shirley and Lote 2005). Eighty to ninety percent of the Al in the plasma bind to proteins, such as transferrin, which affects the kidneys filterability, and lead to an excess of Al gastrointestinal absorption, increased Al blood levels, and further accumulation of this metal in other systems, mainly the central nervous system and the bones (Priest 2004; Shirley and Lote 2005; Bondy 2016; Nie 2018; Rodríguez and Mandalunis 2018).

In this case, the high concentration of Al found in blood (Fig. 1) for the $AlCl_3$ animals could explain the damage in bone structure in this group. The bone accumulation can happen as Al, after its absorption on the body, is able to bind to phosphate groups in the hydroxyapatite crystals (Chappard et al. 2016). In bone tissue, $AlCl_3$ can disturb the calcium and phosphorus metabolism process and decrease the bone mineral density, promoting an imbalance in the bone homeostasis (Li et al. 2011). Studies showed that $AlCl_3$ inactivated Wnt/β-catenin signaling pathway, causing bone cells apoptosis and a bone formation reduction (Sun et al. 2015, 2017). However, reports about the effects in alveolar bone are few.

AB is a highly mineralized and trabecular bone, and although it is only a small percentage of tissue situated surrounding the teeth, it displays a fundamental role dissipating the chewing forces to the rest of the jaw (Zhou et al. 2018). The local occlusion and orthodontic movement and also

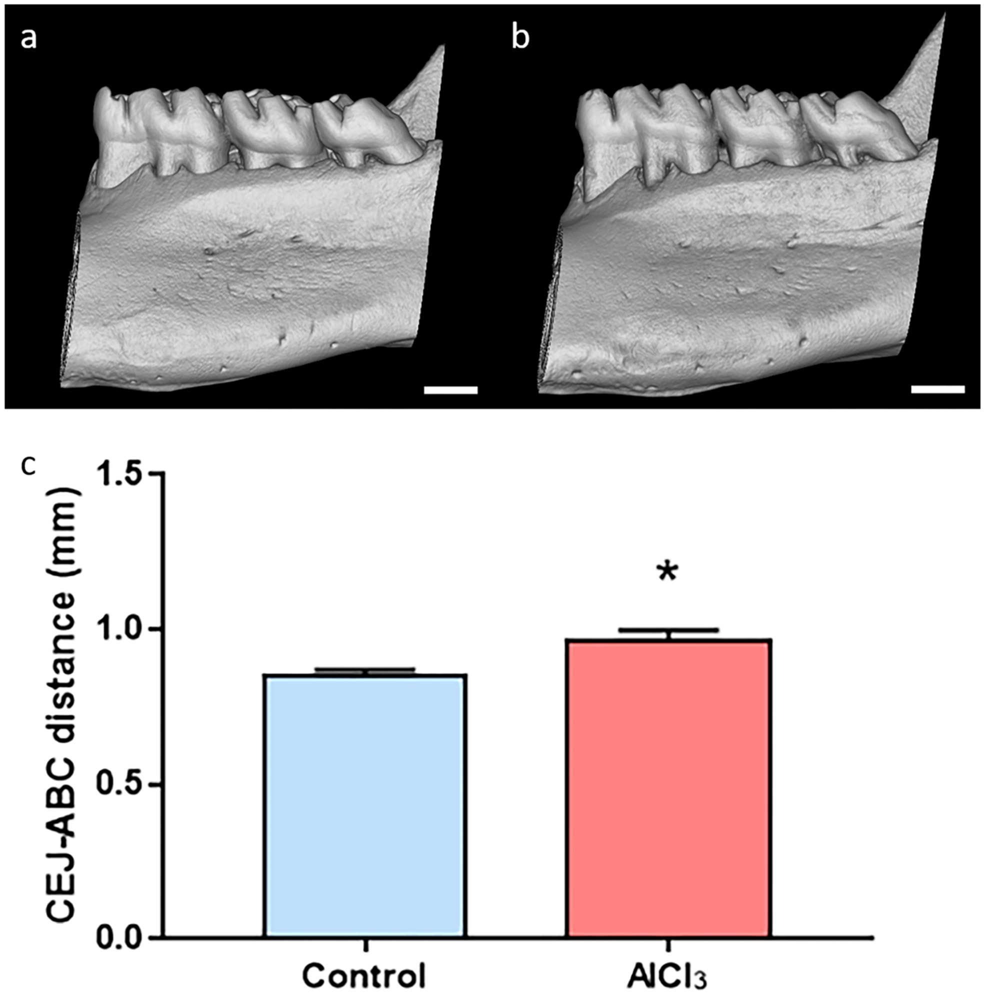

Fig. 6 Effects of $AlCl_3$ exposure (8.3 mg/kg/day) during 60 days on the alveolar bone-loss of rats. In (**a**) and (**b**), three-dimensional representative images of control and aluminum experimental groups, respectively. In (**c**), cementum-enamel junction to alveolar bone crest measured distance (CEJ-ABC distance in mm) of control and $AlCl_3$ animals. Results are expressed as mean ± SEM. Student's *t* test, $*p < 0.05$. Scale bar = 1 mm

systemic factors as hormones and nutrition interfere with the AB remodeling (Krishnan 2006; Zhou et al. 2018). Pathologic features, as periodontitis and osteoporosis, can cause damage related to alveolar bone loss, disrupting not only bone health but also teeth health (Zhou et al. 2018). In this study, the presence of increased concentrations of Al in the animals' blood was related to damage in both composition and microstructure of alveolar bone.

Studies have claimed that Al can affect osteoblasts activity and bone mineralization in the trabecular bone of rats (Rodriguez et al. 1990; Cointry et al. 2005; Yang et al. 2018). Alveolar bone loss has been reported after chronic Al exposure associated to high levels of Al deposited in the alveolar bone (Ferreira et al. 2019). This study corroborates our data, although different doses were used. Our findings are the first to demonstrate changes in the alveolar bone content caused by a dose analogous to human consumption, using vibrational techniques.

Vibrational spectroscopy techniques (infrared and Raman) are interesting tools and have been widely used to characterize bone matrix since its organic and inorganic components present affinity to infrared radiation and scattering of light (Boskey and Mendelsohn 2005; Imbert et al. 2018), providing quantitative and qualitative information about the tissue components and about the mineralization state (Paschalis et al. 2011). FTIR spectroscopy is based upon the absorption of infrared radiation inducing molecules vibrational modes, and those infrared bands can provide information about changes in the spatial distribution of mineral and matrix properties of the samples. It can be used for diagnosing bone diseases related to the bone strength (Nyquist 1997; Turunen et al. 2016).

Our data showed a decrease in different absorbance regions on the average $AlCl_3$ sample spectral. The regions corresponding to phosphate (1100 to 550 cm^{-1}) groups and carbonate (870 cm^{-1}) showed a smaller absorbance in the $AlCl_3$ samples. A decrease in absorbance of those regions was already showed in stress fractured bone (Mata-Miranda et al. 2019). FTIR data also showed a decreased absorbance in the Amide wavelengths (1700 to 1200 cm^{-1}) that are related to collagen. Alterations on the collagen content can also affect the mechanical bone properties, and it may enhance the susceptibility of fractures (Mata-Miranda et al. 2019). As described above, the mineral content could be impaired by the presence of $AlCl_3$. The imbalance between inorganic and organic content in bone tissue may affect the microstructure and function of bone tissue.

Similar to the FTIR analysis, Raman spectroscopy can assess bone quality, but now, the samples are submitted to monochromatic laser light that is inelastically scattered, providing vibrational information of bone biological components (Carden and Morris 2000; Morris and Mandair 2010; Khalid et al. 2018). Raman assessment of bone quality can be used as compositional measure about mineral and collagen state, which implies information about strength and mechanical properties (Morris and Mandair 2010). In our study, mineral crystallinity increased in $AlCl_3$ exposed bone when compared to the control bone. Crystallinity depends on the perfection, size, and strain of the apatite crystalline domains (Farlay et al. 2010). Thereby, variations in crystal dimensions affect bone quality by inducing micro-strain within the apatite lattice [34], and increase of crystallinity is seen in skeletal fluorosis (Roschger 1997) and osteoporotic bone (Boskey et al. 2005; Orkoula 2012).

Carbonate substitutions are common as bone mineralize with the time (Akkus et al. 2004). Those substitutions happen when CO_3^{2-} substitute for OH^- (type A) or PO_4^{3-} (type B) in apatite lattice (Paschalis et al. 2011; Figueiredo et al. 2012) phosphate in osteoporotic (McCreadie et al. 2006), infected (Khalid et al. 2018), and fractured (Mata-Miranda et al. 2019) bone was shown. Our results suggest that type B carbonate substitution is enhanced after $AlCl_3$ chronic exposure, leading to a decrease of AB strength. In Fig. 4b, a decrease observed in exposed AB phosphate levels enhances the loss of phosphate occurrence.

Nanostructure mineral disruptions are intrinsically affiliated with a microscope scale configuration of bone structure (Busse et al. 2013). AB shows a highly mineralized and dense bone mass with large thickness and reduced separation between trabeculae (Zhou et al. 2018). Our MicroCT data showed statistically significantly alterations in exposed samples. Bone mass undergoes a big loss of volume with reduced thickness and number of trabeculae and an increase of trabecula separation after $AlCl_3$ exposure. Such microarchitecture changes highlight the damage caused by the metal toxicity in the bone physical properties.

Alterations in trabeculae parameters and a longer CEJ-ABC distance were already observed in rats with ovariectomy and induced periodontitis (Dai et al. 2015). Our data agrees with the findings previously described, as the animals exposed to $AlCl_3$ also showed a longer CEJ-ABC distance when compared to the control animals, suggesting a worse alveolar bone loss. In periodontology, the alveolar bone loss is an important clinical parameter to evaluate the oral health (Rawlani et al. 2011).

In the literature, alveolar bone loss can be associated to changes in bone metabolism (Dai et al. 2015). Deterioration in bone structure was associated with an increase of mineral-to-matrix ratio and a type B carbonate substitution, which promoted changes in tissue-level mechanical properties of bone aggravating with age (Akkus et al. 2004; Busse et al. 2013; Imbert et al. 2014). Our results are in agreement with those bone metabolism changes, and the alveolar bone loss as an outcome of the Al bone homeostasis disruption can be seen in Fig. 6.

The results of the present study reveal new and interesting findings enlightening aspects in the relationship between aluminum exposure and alveolar bone damage. The high level of Al in the organism is able to promote physical changes in bone components, resulting in microarchitecture conformation changes and alveolar bone loss. Future investigations about mechanical strength bone properties and histological studies showing the cells' behavior with Al intoxication are needed.

Supplementary Information The online version contains supplementary material available at https://doi.org/10.1007/s11356-021-13937-z.

Acknowledgements We thank the Coordenação de Aperfeiçoamento de Pessoal de Nível Superior (CAPES) and the Brazilian National Council for Scientific and Technological Development (CNPq).

Authors' contributions DS-M participated since the beginning of this article idealization, execution of all experiments, and discussion of the data, being guided by RRL during the elaboration of the paper. ROF, LAOL, and LGE contributed in the writing process discussing the mechanisms and environmental importance of aluminum. GSB and FMC contributed to this work executing the X-ray microtomography analysis and contributed for the discussion. RSA was responsible for the technology used in the Fourier transform infrared spectroscopy together with SPAP and ARLA, who also contributed on the writing process. SP was a major contributor for the execution and finalization of this article, contributing with the Raman spectroscopy analysis and the parameters of bone evaluation. CSFM participated on the final writing process, trying to connect the points raised here, suggesting and connecting all the information.

Funding This study was carried out with support from the Programa Nacional de Cooperação Acadêmica na Amazônia – PROCAD/Amazônia da Coordenação de Aperfeiçoamento de Pessoal de Nível Superior – CAPES/Brazil. This research was also supported by the Brazilian National Council for Scientific and Technological Development (CNPq).

Data availability All data generated or analyzed during this study are included in this published article (and its supplementary information files). More specific data and information are available from the corresponding author on reasonable request.

Declarations

Ethics approval and consent to participate All procedures were previously approved by the Ethics committee on animal experimentation by Federal University of Para (under license number CEUA-UFPA 5923210617) following the guidelines suggested by NIH Guide to Care and Use of Laboratory Animals.

Consent for publication Not applicable.

Competing interests The authors declare no competing interests.

References

Agency for Toxic Substances and Disease Registry (ATSDR) (2006) Toxicological profile for aluminum (draft for public comment). U.S. Department of Health and Human Services, Public Health Service, Atlanta

Akkus O, Adar F, Schaffler MB (2004) Age-related changes in physicochemical properties of mineral crystals are related to impaired mechanical function of cortical bone. Bone 34(3):443–453. https://doi.org/10.1016/j.bone.2003.11.003

Balbinot G, Leitune VCB, Ponzoni D, Collares FM (2019a) Bone healing with niobium-containing bioactive glass composition in rat femur model: a micro-CT study. Dent Mater 35:1490–1497. https://doi.org/10.1016/j.dental.2019.07.012

Balbinot G, Collares FM, Herpich TL, Visioli F, Samuel SMW, Leitune VCB (2019b) Niobium containing bioactive glasses as remineralizing filler for adhesive resins. Dent Mater 36:221–228. https://doi.org/10.1016/j.dental.2019.11.014

Becaria A, Lahiri DK, Bondy SC, Chen D, Hamadeh A, Li H, Taylor R, Campbell A (2006) Aluminum and copper in drinking water enhance inflammatory or oxidative events specifically in the brain. J Neuroimmunol 176(1-2):16–23. https://doi.org/10.1016/j.jneuroim.2006.03.025

Bojórquez-Quintal E, Escalante-Magaña C, Echevarría-Machado I, Martínez-Estévez M (2017) Aluminum, a friend or foe of higher plants in acid soils. Front Plant Sci 8. https://doi.org/10.3389/fpls.2017.01767

Bondy SC (2016) Low levels of aluminum can lead to behavioral and morphological changes associated with Alzheimer's disease and age-related neurodegeneration. NeuroToxicology 52:222–229. https://doi.org/10.1016/j.neuro.2015.12.002

Boskey AL, Mendelsohn R (2005) Infrared spectroscopic characterization of mineralized tissues. Vib Spectrosc 38(1-2):107–114. https://doi.org/10.1016/j.vibspec.2005.02.015

Boskey AL, DiCarlo E, Paschalis E, West P, Mendelsohn R (2005) Comparison of mineral quality and quantity in iliac crest biopsies from high- and low-turnover osteoporosis: an FT-IR microspectroscopic investigation. Osteoporos Int 16(12):2031–2038. https://doi.org/10.1007/s00198-005-1992-3

Busse B, Bale HA, Zimmermann EA, Panganiban B, Barth HD, Carriero A et al (2013) Vitamin D deficiency induces early signs of aging in human bone, increasing the risk of fracture. Sci Transl Med 5(193):193ra88–193ra88. https://doi.org/10.1126/scitranslmed.3006286

Carden A, Morris MD (2000) Application of vibrational spectroscopy to the study of mineralized tissues (review). J Biomed Opt 5(3):259–268. https://doi.org/10.1117/1.429994

Chappard D, Bizot P, Mabilleau G, Hubert L (2016) Aluminum and bone: review of new clinical circumstances associated with Al3+ deposition in the calcified matrix of bone. Morphologie 100(329):95–105. https://doi.org/10.1016/j.morpho.2015.12.001

Chappard D, Mabilleau G, Masson C, Tahla A, Legrand E (2018) Metaplastic woven bone in bone metastases: a Fourier-transform infrared analysis and imaging of bone quality (FTIR). Morphologie 102(337):69–77. https://doi.org/10.1016/j.morpho.2018.02.002

Cheng C (2016) Spectral and morphological classification of different chronic and acute Taiwanese gallstones via FTIR, SEM and ESEM-EDX microanalyses. Dig Liver Dis 48(5):519–527. https://doi.org/10.1016/j.dld.2016.01.010

Chu T, Liu S, Babler W (2014) Craniofacial biology, orthodontics, and implants. Basic Appl Bone Biol:225–242. https://doi.org/10.1016/b978-0-12-416015-6.00011-3

Cointry GR, Capozza RF, Negri AL, Ferretti JL (2005) Biomechanical impact of aluminum accumulation on the pre- and post-yield behavior of rat cortical bone. J Bone Miner Metab 23(1):15–23. https://doi.org/10.1007/s00774-004-0535-x

Colomina MT, Peris-Sampedro F (2017) Aluminum and Alzheimer's disease. Adv Neurobiol 8:183–197. https://doi.org/10.1007/978-3-319-60189-2_9

Costa N, Correa R, Júnior I, Figueiredo A, Vilhena K, Farias-Junior P, Teixeira F, Ferreira N, Pereira-Júnior J, Dantas K, Silva M, Silva-Junior A, Alves-Junior S, Pinheiro J, Lima R (2014) Physical, chemical, and immunohistochemical investigation of the damage to salivary glands in a model of intoxication with aluminium citrate. Int J Environ Res Public Health 11(12):12429–12440. https://doi.org/10.3390/ijerph111212429

Dai J, Ma Y, Shi M, Cao Z, Zhang Y, Miron RJ (2015) Initial changes in alveolar bone volume for sham-operated and ovariectomized rats in ligature-induced experimental periodontitis. Clin Oral Investig 20(3):581–588. https://doi.org/10.1007/s00784-015-1531-3

Doube M, Kłosowski MM, Arganda-Carreras I, Cordelières FP, Dougherty RP, Jackson JS, Schmid B, Hutchinson JR, Shefelbine SJ (2010) BoneJ: Free and extensible bone image analysis in ImageJ. Bone 47(6):1076–1079. https://doi.org/10.1016/j.bone.2010.08.023

Driscoll CT, Schecher WD (1990) The chemistry of aluminum in the environment. Environ Geochem Health 12(1-2):28–49. https://doi.org/10.1007/bf01734046

European Food Safety Authority (2013) Dietary exposure to aluminium-containing food additives. Supporting Publications 10(4):EN-411, 17. https://doi.org/10.2903/sp.efsa.2013.EN-411

Exley C (2013) Human exposure to aluminium. Environ Sci Process Impacts 15(10):1807–1816. https://doi.org/10.1039/c3em00374d

Farlay D, Panczer G, Rey C, Delmas PD, Boivin G (2010) Mineral maturity and crystallinity index are distinct characteristics of bone mineral. J Bone Miner Metab 28(4):433–445. https://doi.org/10.1007/s00774-009-0146-7

Fernandes PG (2014) Aplicação da Microtomografia Computadorizada para a Análise Morfométrica Bi e Tridimensional na Avaliação da Perda óssea Experimental em Ratos. PhD thesis, Faculdade de Ribeirão Preto da Universidade de São Paulo

Ferreira N, Costa N, Leão L, Puty B, Fernandes R, Silva-Júnior A et al (2019) Effects of exposure to aluminum citrate in a model of induced alveolar bone loss in rats. Indian J Exp Biol 57:282–287

Figueiredo MM, Gamelas JAF, Martins AG (2012) Characterization of bone and bone-based graft materials using FTIR spectroscopy. Infrared spectroscopy-life and biomedical sciences 315–338. https://doi.org/10.5772/36379

Gherardi RK, Aouizerate J, Cadusseau J, Yara S, Authier FJ (2016) Aluminum adjuvants of vaccines injected into the muscle: normal fate, pathology and associated disease. Morphologie 100(329):85–94. https://doi.org/10.1016/j.morpho.2016.01.002

Goudouri O, Kontonasaki E, Boccaccini AR (2017) Layered scaffolds for periodontal regeneration. Biomaterials for Oral and Dental Tissue Engineering 279–295. https://doi.org/10.1016/b978-0-08-100961-1.00017-7

Gouléa JP, Grangeot-Keros L (2019) Aluminum and vaccines: current state of knowledge. Med Mal Infect 50:16–21. https://doi.org/10.1016/j.medmal.2019.09.012

Hirshi J (2006) Virtual fabrication of aluminium products. Wiley-VCH Verlag, Weinheim

Imbert L, Aurégan J, Pernelle K, Hoc T (2014) Mechanical and mineral properties of osteogenesis imperfecta human bones at the tissue level. Bone 65:18–24. https://doi.org/10.1016/j.bone.2014.04.030

Imbert L, Gourion-Arsiquaud S, Villarreal-Ramirez E, Spevak L, Taleb H, van der Meulen MCH, Mendelsohn R, Boskey AL (2018) Dynamic structure and composition of bone investigated by nanoscale infrared spectroscopy. PLoS One 13(9):e0202833. https://doi.org/10.1371/journal.pone.0202833

Khalid M, Bora T, Ghaithi AA, Thukral S, Dutta J (2018) Raman spectroscopy detects changes in bone mineral quality and collagen cross-linkage in Staphylococcus infected human bone. Sci Rep 8(1):9417. https://doi.org/10.1038/s41598-018-27752-z

Kinane DF, Stathopoulou PG, Papapanou PN (2017) Periodontal diseases. Nat Rev Dis Primers 3:17038. https://doi.org/10.1038/nrdp.2017.38

Klotz K, Weistenhöfer W, Neff F, Hartwig A, van Thriel C, Drexler H (2017) The health effects of aluminum exposure. Dtsch Arztebl Online. https://doi.org/10.3238/arztebl.2017.0653

Krishnan V (2006) Regulation of bone mass by Wnt signaling. J Clin Investig 116(5):1202–1209. https://doi.org/10.1172/jci28551

Kumar V, Gill KD (2014) Oxidative stress and mitochondrial dysfunction in aluminium neurotoxicity and its amelioration: a review. NeuroToxicology 41:154–166. https://doi.org/10.1016/j.neuro.2014.02.004

Lewis L, Carson S, Bydder S, Athifa M, Williams AM, Bremner A (2014) Evaluating the effects of aluminum-containing and non-aluminum containing deodorants on axillary skin toxicity during radiation therapy for breast cancer: a 3-armed randomized controlled trial. Int J Radiat Oncol Biol Phys 90(4):765–771. https://doi.org/10.1016/j.ijrobp.2014.06.054

Li X, Hu C, Zhu Y, Sun H, Li Y, Zhang Z (2011) Effects of aluminum exposure on bone mineral density, mineral, and trace elements in rats. Biol Trace Elem Res 143(1):378–385

Ligt R, van Duijn E, Grossouw D, Bosgra S, Burggraaf J, Windhorst A et al (2018) Assessment of dermal absorption of aluminum from a representative antiperspirant formulation using a 26Al microtracer approach. Clin Transl Sci 11:573–581. https://doi.org/10.1111/cts.12579

Lin Y, Shih Y, Chen C, Fang C (2018) Aluminum salts as an adjuvant for pre-pandemic influenza vaccines: a meta-analysis. Sci Rep 8(1):11460. https://doi.org/10.1038/s41598-018-29858-w

Martinez CS, Alterman CDC, Peçanha FM, Vassallo DV, Mello-Carpes PB, Miguel M, Wiggers GA (2016) Aluminum exposure at human dietary levels for 60 days reaches a threshold sufficient to promote memory impairment in rats. Neurotox Res 31(1):20–30. https://doi.org/10.1007/s12640-016-9656-y

Mata-Miranda MM, Guerrero-Ruiz M, Gonzalez-Fuentes JR, Hernandez-Toscano CM, Garcia-Andino JR, Sanchez-Brito M et al (2019) Characterization of the biological fingerprint and identification of associated parameters in stress fractures by FTIR spectroscopy. Biomed Res Int:1–10. https://doi.org/10.1155/2019/1241452

McCreadie BR, Gamelas JAF, Martins AG (2006) Bone tissue compositional differences in women with and without osteoporotic fracture. Bone 39(6):1190–1195. https://doi.org/10.1016/j.bone.2006.06.008

Morris MD, Mandair GS (2010) Raman assessment of bone quality. Clin Orthop Relat Res 469(8):2160–2169. https://doi.org/10.1007/s11999-010-1692-y

Nie J (2018) Exposure to aluminum in daily life and Alzheimer's disease. In Neurotoxicity of Aluminum (pp. 99-111). Springer, Singapore. https://doi.org/10.1007/978-981-13-1370-7_6

Niu Q (2018) Overview of the Relationship Between Aluminum Exposure and Health of Human Being. Adv Exp Med Biol 1091:1–31. https://doi.org/10.1007/978-981-13-1370-7_1

Nyquist RA (1997) Infrared and Raman spectral atlas of inorganic and organic salts, vol 1-3. Academic Press, Cambridge

Orkoula MG (2012) Study of bone matrix changes induced by osteoporosis in rat tibia using Raman spectroscopy. Vib Spectrosc 63:404–408. https://doi.org/10.1016/j.vibspec.2012.09.016

Paschalis EP, Mendelsohn R, Boskey AL (2011) Infrared assessment of bone quality: a review. Clin Orthop Relat Res 469(8):2170–2178. https://doi.org/10.1007/s11999-010-1751-4

Priest ND (2004) The biological behaviour and bioavailability of aluminium in man, with special reference to studies employing aluminium-26 as a tracer: review and study update. J Environ Monit 6(5):375–403. https://doi.org/10.1039/b314329p

Principi N, Esposito S (2018) Aluminum in vaccines: does it create a safety problem? Vaccine. 36:5825–5831. https://doi.org/10.1016/j.vaccine.2018.08.036

Rawlani SM, Rawlani S, Degwekar S, Bhowte RR, Motwani M (2011) Oral health status and alveolar bone loss in treated leprosy patients of central India. Indian J Lepr 83(4):215–224

Reagan-Shaw S, Nihal M, Ahmad N (2008) Dose translation from animal to human studies revisited. FASEB J 22(3):659–661. https://doi.org/10.1096/fj.07-9574lsf

Rodríguez J, Mandalunis PM (2018) A review of metal exposure and its effects on bone health. J Toxicol 2018:1–11. https://doi.org/10.1155/2018/4854152

Rodriguez M, Felsenfeld AJ, Llach F (1990) Aluminum administration in the rat separately affects the osteoblast and bone mineralization. J Bone Miner Res 5(1):59–67. https://doi.org/10.1002/jbmr.5650050110

Roschger P (1997) Mineralization of cancellous bone after alendronate and sodium fluoride treatment: a quantitative backscattered electron imaging study on minipig ribs. Bone 20:393–397

Salusky IB, Foley J, Nelson P, Goodman WG (1991) Aluminum accumulation during treatment with aluminum hydroxide and dialysis in children and young adults with chronic renal disease. N Engl J Med 324(8):527–531. https://doi.org/10.1056/NEJM199102213240804

Schifman RB, Luevano DR (2018) Aluminum toxicity: evaluation of 16-year trend among 14 919 patients and 45 480 results. Arch Pathol Lab Med 142(6):742–746. https://doi.org/10.5858/arpa.2017-0049-OA

Sharma DR, Sunkaria A, Wani WY, Sharma RK, Kandimalla RJL, Bal A, Gill KD (2013) Aluminium induced oxidative stress results in decreased mitochondrial biogenesis via modulation of PGC-1α expression. Toxicol Appl Pharmacol 273(2):365–380. https://doi.org/10.1016/j.taap.2013.09.012

Shirley DG, Lote CJ (2005) Renal handling of aluminium. Nephron Physiol 101(4):99–103. https://doi.org/10.1159/000088331

Souza-Monteiro D, Oliveira NPB, Oliveira FR, Eiró LG, Bittencourt LO, Santos CV et al (2020) Aluminum-induced toxicity in salivary glands of mice after long-term exposure: insights into the redox state and morphological analyses. Biol Trace Elem Res 198:575–582. https://doi.org/10.1007/s12011-020-02091-1

Sun X, Cao Z, Zhang Q, Liu S, Xu F, Che J, Zhu Y, Li Y, Pan C, Liang W (2015) Aluminum trichloride impairs bone and downregulates Wnt/β-catenin signaling pathway in young growing rats. Food Chem Toxicol 86:154–162. https://doi.org/10.1016/j.fct.2015.10.005

Sun X, Wang H, Huang W, Yu H, Shen T, Song M, Han Y, Li Y, Zhu Y (2017) Inhibition of bone formation in rats by aluminum exposure via Wnt/β-catenin pathway. Chemosphere 176:1–7. https://doi.org/10.1016/j.chemosphere.2017.02.086

Totten GE, MacKenzie DS (eds) (2003) Handbook of aluminum, vol. 1: physical metallurgy and processes. CRC press

Turunen MJ, Kaspersen JD, Olsson U, Guizar-Sicairos M, Bech M, Schaff F, Tägil M, Jurvelin JS, Isaksson H (2016) Bone mineral crystal size and organization vary across mature rat bone cortex. J Struct Biol 195(3):337–344. https://doi.org/10.1016/j.jsb.2016.07.005

Willhite CC, Karyakina NA, Yokel RA, Yenugadhati N, Wisniewski TM, Arnold IMF, Momoli F, Krewski D (2014) Systematic review of potential health risks posed by pharmaceutical, occupational and consumer exposures to metallic and nanoscale aluminum, aluminum oxides, aluminum hydroxide and its soluble salts. Crit Rev Toxicol 44:1–80. https://doi.org/10.3109/10408444.2014.934439

Yang X, Yu K, Wang H, Zhang H, Bai C, Song M, Han Y, Shao B, Li Y, Li X (2018) Bone impairment caused by AlCl3 is associated with activation of the JNK apoptotic pathway mediated by oxidative stress. Food Chem Toxicol 116:307–314. https://doi.org/10.1016/j.fct.2018.04.057

Yokel RA, Hics CL, Florence RL (2008) Aluminum bioavailability from basic sodium aluminum phosphate, an approved food additive emulsifying agent, incorporated in cheese. Food Chem Toxicol 46(6): 2261–2266. https://doi.org/10.1016/j.fct.2008.03.004

Zhou S, Yang Y, Ha N, Zhang P, Ma X, Gong X, Hong Y, Yang X, Yang S, Dai Q, Jiang L (2018) The specific morphological features of alveolar bone. J Craniofac Surg 1:1216–1219. https://doi.org/10.1097/scs.0000000000004395

Publisher's note Springer Nature remains neutral with regard to jurisdictional claims in published maps and institutional affiliations.